

Aqueous-phase hydrogenation and hydrodeoxygenation of biomass-derived oxygenates with bimetallic catalysts†

Cite this: *Green Chem.*, 2014, **16**, 708

Jechan Lee, Yong Tae Kim and George W. Huber*

The reaction rate on a per site basis for aqueous-phase hydrogenation (APH) of propanal, xylose, and furfural was measured over various alumina-supported bimetallic catalysts (Pd–Ni, Pd–Co, Pd–Fe, Ru–Ni, Ru–Co, Ru–Fe, Pt–Ni, Pt–Co, and Pt–Fe) using a high-throughput reactor (HTR). The results in this paper demonstrate that the activity of bimetallic catalysts for hydrogenation of a carbonyl group can be 110 times higher than monometallic catalysts. The addition of Fe to a Pd catalyst increased the activity for hydrogenation of propanal, xylose, and furfural. The Pd₁Fe₃ catalyst had the highest reaction rate for APH of propanal among all catalysts tested in the HTR. The addition of Fe to the Pd catalyst increased the reaction rate for xylose hydrogenation by a factor of 51, compared to the monometallic Pd catalyst. However, no bimetallic catalyst tested in this study was more active than the monometallic Ru catalyst for hydrogenation of xylose. The Pd₁Fe₃ catalyst had the highest reaction rate for APH of furfural, which was 9 times higher than the rate of the Pd catalyst. The Pd₁Fe₃/Zr–P, a bimetallic bifunctional catalyst, was 14 times more active on a per site basis than a Pd/Zr–P catalyst for aqueous-phase hydrodeoxygenation (HDO) of sorbitol in a continuous flow reactor. The addition of Fe to the Pd catalyst increased the rate of C–C cleavage reactions and promoted the conversion of sorbitan and isosorbide in HDO of sorbitol. Pd₁Fe₃/Zr–P also had a higher yield of gasoline-range products than the Pd/Zr–P catalyst.

Received 5th June 2013,
Accepted 6th January 2014
DOI: 10.1039/c3gc41071d
www.rsc.org/greenchem

1. Introduction

Aqueous-phase hydrogenation (APH) reactions, a critical fundamental reaction of aqueous-phase processing (APP), are used in a variety of processes for the conversion of biomass into fuels and chemicals.^{1–7} APH involves the hydrogenation of a range of functionalities including aldehydes, ketones, furans, carbohydrates, and alkenes.^{8–10}

Bimetallic catalysts often have a higher activity than either of their parent metals.¹¹ For example, Co and Ni promoted Pt catalysts exhibited a higher activity for the hydrogenation of C=O bonds than the corresponding monometallic catalysts.^{12,13} A bimetallic Ni–Pd catalyst was more active than RANEY® Ni for the hydrogenation of HMF and furfural.¹⁴ The addition of Ni, Co, and Fe to a Pt catalyst increased the activity for aqueous-phase reforming (APR) of ethylene glycol up to 3 times.¹⁵ It was proposed that this increase in catalytic activity was because the Ni, Co, and Fe decrease the adsorption energy

of carbon monoxide (CO) and H on the Pt metal surface.^{16–19} Bimetallic catalysts have also been shown to have a higher activity for electrocatalytic reactions.^{20–24} For example, Pt–Ru bimetallic catalyst was more active than monometallic Pt catalyst for electrocatalytic oxidation of glycerol.²⁴

Bimetallic catalysts can also modify the reaction selectivity.¹¹ For instance, Pd–Cu and Ni–Fe bimetallic catalysts had a higher selectivity toward hydrogenation products but lower selectivity toward decarbonylation products for furfural conversion than the pure monometallic Pd and Ni catalysts.^{25,26} Pt–Ni and Pt–Co bimetallic catalysts showed a higher selectivity toward deoxygenation products than monometallic Pt catalyst for hydrodeoxygenation (HDO) of *meta*-cresol.²⁷ The addition of Sn to Ni catalysts can increase the hydrogen selectivity from 47% to 93% for APR of ethylene glycol.²⁸ In spite of the clear advantages of bimetallic catalysts, they have not been widely used for biomass conversion reactions. More information about the use of bimetallic catalysts for fundamental reactions like APH reactions of model biomass compounds is needed to properly design bimetallic catalytic processes for realistic biomass conversion processes.

High-throughput techniques have been developed that make possible the rapid screening of large numbers of catalytic materials.^{10,15,29–33} We have previously used a high-

Department of Chemical and Biological Engineering, University of Wisconsin–Madison, 1415 Engineering Drive, Madison, Wisconsin 53706, USA.

E-mail: huber@engr.wisc.edu

†Electronic supplementary information (ESI) available. See DOI: 10.1039/c3gc41071d

throughput reactor (HTR) to measure the initial activity for APH and hydrogenolysis of model biomass compounds, including acetaldehyde, propanal, acetone, xylose, furfural, furfuryl alcohol, tetrahydrofurfuryl alcohol (THFA), and xylitol, with monometallic catalysts.¹⁰ We observed that the reaction rate for hydrogenation of a carbonyl group is dependent on both the metal surface and the functionality that surrounds the carbonyl group.¹⁰ Results obtained from the HTR are also consistent with results obtained from a continuous electrocatalytic membrane reactor.³⁴ The objective of this paper is to develop relationships between the reaction rate for hydrogenation of different feed molecules containing a carbonyl group and different bimetallic catalysts to get insight into which bimetallic catalytic systems might be useful for aqueous-phase conversion of more complicated biomass molecules. We then take one of the most promising bimetallic catalysts obtained from high-throughput studies and test it for HDO of sorbitol.

2. Experimental

2.1. Catalyst preparation

Gamma-alumina (γ -Al₂O₃, $S_{\text{BET}} = 142 \text{ m}^2 \text{ g}^{-1}$) was used as a support of the catalysts tested in the HTR. The γ -Al₂O₃ was formed by calcination of Boehmite (Catapal® A Alumina, Sasol North America Inc.) at 873 K (heating rate: 20 K min⁻¹) for 4 hours in static air. 3 wt% Pd, Pt, and Ru catalysts were prepared by incipient wetness impregnation with aqueous solutions of the following metal precursors: Pd(NH₃)₄(NO₃)₂, Pt(NH₃)₄(NO₃)₂, and Ru(NO)(NO₃)₃ (Strem Chemicals). 20 wt% Ni, Co, and Fe catalysts were prepared by incipient wetness impregnation with aqueous solutions of the following metal precursors: Ni(NO₃)₂·6H₂O, Co(NO₃)₂·6H₂O, and Fe(NO₃)₃·9H₂O (Sigma-Aldrich). After incipient wetness impregnation, the metal salt solution-support mixture was dried at 373 K for 12 hours. The dried catalysts were calcined at 523 K (20 K min⁻¹; for Pd and Pt catalysts) and 823 K (20 K min⁻¹; for Ni, Co, and Fe catalysts) for 4 hours in static air. The Ru catalyst reduced at 523 K (1 K min⁻¹) under H₂ flow (40 mL min⁻¹, Airgas 99.99%) for 2 hours without calcination, followed by purging with helium (He) flow (40 mL min⁻¹, Airgas 99.995%) for 2 hours.

To prepare the γ -Al₂O₃ supported bimetallic catalysts, the metal salts of Ni, Co, and Fe (Ni(NO₃)₂·6H₂O, Co(NO₃)₂·6H₂O, and Fe(NO₃)₃·9H₂O (Sigma-Aldrich)) were added to the prepared 3 wt% Pd/ γ -Al₂O₃, Ru/ γ -Al₂O₃, and Pt/ γ -Al₂O₃ catalysts by incipient wetness impregnation. After incipient wetness impregnation, the base metal salt solution-noble metal catalyst mixture was dried at 373 K for 12 hours and then calcined at 523 K (20 K min⁻¹) for 4 hours in static air.

Zirconium phosphate (Zr-P, $S_{\text{BET}} = 361 \text{ m}^2 \text{ g}^{-1}$, total pore volume = 1.05 cm³ g⁻¹) was prepared by co-precipitation using 1.0 mol L⁻¹ of ZrCl₂·8H₂O (Aldrich) and 1.0 mol L⁻¹ of NH₄H₂PO₄ (Aldrich) aqueous solutions at a molar ratio of P/Zr = 2, as described by Kamiya *et al.*³⁵ The precipitate was aged at room temperature for 30 minutes, filtered, washed

with deionized water until the pH was 5, dried at 373 K for 12 hours, and then calcined at 673 K (20 K min⁻¹) for 4 hours in static air. A 3 wt% Pd/Zr-P catalyst was prepared by incipient wetness impregnation with an aqueous solution of Pd(NH₃)₄(NO₃)₂ (Strem Chemicals). The Pd/Zr-P catalyst was calcined at 523 K (20 K min⁻¹) for 3 hours in static air. A Pd-Fe/Zr-P bimetallic catalyst with a Fe to Pd molar ratio of 3 : 1 (Pd₁Fe₃/Zr-P) was prepared by sequentially impregnating the 3 wt% Pd/Zr-P catalyst dried at 373 K with an aqueous solution of Fe(NO₃)₃·9H₂O (Sigma-Aldrich). The Pd-Fe/Zr-P catalyst was calcined at 523 K (20 K min⁻¹) for 3 hours in static air.

2.2. Catalyst characterization

Static H₂ chemisorption was carried out in a Quantachrome Autosorb iQ Automated Gas Sorption system. Before H₂ chemisorption, catalysts were reduced *in situ* under H₂ flow up to 573 K (1 K min⁻¹), held for 2 hours, purged with He for 2 hours, evacuated for 140 minutes, and cooled down to room temperature. Hydrogen was dosed on the catalyst until the equilibrium pressure was 560 mmHg. The hydrogen in the cell was then evacuated at room temperature, and again hydrogen was dosed on the catalyst to determine the amount of weakly adsorbed hydrogen. The amount of strongly adsorbed hydrogen was determined by subtracting the second isotherm from the first one.

Pulse CO chemisorption was conducted in a Micromeritics AutoChem II 2920 unit equipped with a thermal conductivity detector (TCD) to measure the consumption of CO. Before CO chemisorption, catalysts were reduced *in situ* under H₂ flow up to 573 K (1 K min⁻¹), held for 2 hours, and cooled down to room temperature. The chemisorption was carried out at 300 K in a 50 mL min⁻¹ stream of He using a pulse chemisorption technique, in which 500 mL pulses of 10% CO/He were utilized.

Temperature programmed reduction (TPR) was performed in a flow of 10% H₂/Ar mixture gas at a flow rate of 50 mL min⁻¹ with a temperature ramp of 10 K min⁻¹. A dry ice/acetone cooling bath removed moisture from TPR effluent stream at 195 K before the TCD. Before a TPR run, catalysts were pretreated in He at 423 K for 30 minutes. The consumption of H₂ was monitored using the TCD of the Micromeritics AutoChem II 2920 unit and quantified based on H₂ consumption during TPR of AgO as standard.

Brunauer-Emmett-Teller (BET) surface areas of the Pd/Zr-P and Pd-Fe/Zr-P catalysts were calculated from nitrogen adsorption data at 77 K obtained using a Micromeritics ASAP 2020 system. Before the measurements, the sample was degassed under vacuum at 523 K.

The bulk crystalline structure of the Pd/Zr-P and Pd-Fe/Zr-P catalysts was determined by X-ray diffraction (XRD). XRD patterns were obtained with a Scintag Pad V using Cu K α radiation ($k = 0.15406 \text{ nm}$), operated at 45 kV and 40 mA (2.0 kW) at a scan rate of 0.2° (2 θ) s⁻¹. Each sample was reduced at 573 K for 2 hours in H₂ and passivated prior to XRD experiments. The assignment of the crystalline phases was carried

out using JADE 9.0 software package (Rigaku) for the ICDD database.

2.3. High-throughput studies

APH of propanal, xylose, and furfural over different bimetallic catalysts were carried out in a HTR manufactured by HEL Group (Model # CAT24). This HTR reactor consisted of 24 wells machined into a cylindrical stainless steel high pressure chamber. Stainless steel cooling tips were inserted into the top of each glass tube reactor which put in each well in the HTR, preventing the mixing of vapor between the glass tube reactors. WinIso E670 system software controlled and monitored the system temperature, pressure, gas flow rate, and stirring speed. In this study, we have used the HTR to measure the reaction rate, not deactivation or regeneration tests.

For a run, each catalyst was typically put into two different random wells to measure the effect of cross-talk between wells. We could not detect severe cross-talk between wells in a run. Each catalyst was tested three to five times.

Ten mg of each catalyst was loaded into each well in the HTR and then the monometallic Pd, Ru, and Pt catalysts and all bimetallic catalysts were reduced at 573 K (1 K min^{-1}) and the monometallic Ni, Co, and Fe catalysts were reduced at 673 K (1 K min^{-1}) in H_2 (50 mL min^{-1} , Airgas 99.99%) for 2 hours at ambient pressure and purged with He (50 mL min^{-1} , Airgas 99.995%) for 30 minutes. After reduction, the catalysts were cooled to room temperature under He flow, then sealed with closed valves, and transported to the glove box. In the glove box, the HTR head was removed, magnetic stir bars were placed into each glass tube reactor which was loaded into the high pressure chamber, and 2 mL of an aqueous feedstock solution was added to each of the glass tube reactors with a micropipette. The HTR was then put on the heating block and pressurized with H_2 to 4.38 MPa. After the reactor was pressurized, the temperature was increased at a rate of 20 K min^{-1} . After the HTR was heated to the reaction temperature and then pressurized to 5.41 MPa. A stirring speed of 800 rpm was used during the reaction. We checked that there was no external mass transfer limitation at 800 rpm in the HTR.¹⁰

Once a reaction set finished, the HTR was removed from the heater and cooled down to room temperature in an ice bath at a rate of around 14 K min^{-1} . After reaching room temperature, the HTR was depressurized to atmospheric pressure, and samples in each well were taken by a 3 mL syringe and filtered with a syringe filter ($0.2 \mu\text{m}$). The samples from APH of propanal and furfural were analyzed by a gas chromatograph (GC; Agilent 7890A) using a flame ionization detector (FID) with Rtx®-VMS (Restek, Catalog no. 19915) capillary column. A high-performance liquid chromatography (HPLC; Shimadzu LC-20AT) with ultraviolet-visible (UV-Vis; SPD-20AV) and RID (RID-10A) detectors was used to analyze the samples from APH of xylose.

The average conversion of each catalyst for APH reactions performed in this study is shown in Table S1.†

The reaction rate (based on H_2 uptake of fresh catalyst) was calculated by the equation:

$$\text{Reaction rate (h}^{-1}\text{)} = \frac{\sum (\text{moles of product})}{(\text{H}_2 \text{ uptake}) \times S \times (\text{g of catalyst}) \times (\text{reaction time})}$$

where S is the number of surface metal atoms adsorbed by hydrogen. We assumed that hydrogen was dissociatively adsorbed on all metal surfaces so $S = 2$. During all experiments, the carbon balance was higher than 90% (see Table S1†). The carbon balance was calculated by the equation:

$$\text{Carbon balance (\%)} = 100 \times \frac{\text{moles of carbon out (detected by GC)}}{\text{moles of carbon in}}$$

2.4. Continuous-flow reactor studies

HDO of sorbitol was conducted in a stainless-steel tubular flow reactor (30 cm long, 6.35 mm of outer diameter), heated by a furnace (Thermcraft Inc. no. 114-12-1ZH). Reactants including 20 wt% sorbitol solution and hydrogen gas were flowing upwardly. A uniform temperature profile along the catalyst bed was achieved using aluminum filler inserted in the void between the furnace and the tubular reactor. For catalytic activity measurements, 3.3 g of the catalyst without diluents was loaded into the reactor with glass wool packed on both sides. Before the reaction, the catalyst was reduced *in situ* under H_2 flow (128 mL min^{-1}) at 573 K (1 K min^{-1}) for 2 hours. After the reduction was complete, the furnace was cooled to the desired reaction temperature and the reactor system was pressurized to 6.21 MPa using a back-pressure regulator. A 20 wt% sorbitol solution was then fed to the reactor using an Eldex Laboratories 1SM HPLC pump with co-fed H_2 (40 mL min^{-1}). A stainless-steel gas-liquid separator (150 mL) was used to accumulate liquid products at the top of the reactor. The gaseous products continued to flow to the back-pressure regulator to maintain the reaction pressure. Both an excess flow shut-off valve (Parker Hannifin Corporation, FS190) and a pressure relief valve (Swagelok®, SS-4R3A) were also installed in the reactor system to ensure safe operation. Online GC (Agilent 7890A) was used to analyze the reactor effluent gas. Carbon dioxide (CO_2) and CO in the gaseous products were analyzed using a TCD with a GS-Carbon PLOT (Agilent, Catalog no. 113-3133) capillary column. Alkanes in the gaseous products were analyzed using a FID with Rt®-Q-Bond (Restek, Catalog no. 19744) capillary column. The liquid product accumulated in the gas-liquid separator was drained periodically into a collecting container in which cyclohexane (Acros Organics, 99%) was preloaded, and passed through a $0.2 \mu\text{m}$ syringe filter. The aqueous phase and organic phase were analyzed using GC-MS (Shimadzu GC-2010), offline GC-FID (Agilent 7890A) with Rtx®-VMS (Restek, Catalog no. 19915) capillary column, and HPLC (Shimadzu LC-20AT) with UV-Vis (SPD-20AV) and RID (RID-10A) detectors. In HDO of sorbitol, conversion, molar carbon selectivity, yield, and turnover frequency (TOF) were calculated according to the

following equations:

Mavrikakis demonstrated that hydrogen binds weaker on Fe/Pd alloy than Pd metal.⁴¹

$$\text{Conversion (\%)} = 100 \times \frac{C_{\text{sorbitol,inlet}} V_{\text{inlet}} - C_{\text{sorbitol,aqueous}} V_{\text{aqueous}}}{C_{\text{sorbitol,inlet}} V_{\text{inlet}}}$$

$$\text{Molar carbon selectivity (\%)} = 100 \times \frac{C_{\text{product,aqueous}} V_{\text{aqueous}} + C_{\text{product,organic}} V_{\text{organic}} + C_{\text{product,gaseous}} V_{\text{gaseous}}}{C_{\text{sorbitol,inlet}} V_{\text{inlet}} - C_{\text{sorbitol,aqueous}} V_{\text{aqueous}}}$$

$$\text{Yield (\%)} = 100 \times \frac{C_{\text{product,aqueous}} V_{\text{aqueous}} + C_{\text{product,organic}} V_{\text{organic}} + C_{\text{product,gaseous}} V_{\text{gaseous}}}{C_{\text{sorbitol,inlet}} V_{\text{inlet}}}$$

$$\text{Turnover frequency (h}^{-1}\text{)} = \frac{(\text{molar sorbitol flow rate}) \times (\text{conversion}/100)}{(\text{H}_2 \text{ uptake after reaction}) \times 2 \times (\text{g of catalyst})}$$

where $C_{\text{sorbitol,inlet}}$ and $C_{\text{sorbitol,aqueous}}$ are the concentration of sorbitol at the inlet and outlet, respectively; C_{product} is the concentration of carbon in the product at the corresponding phase; V is the corresponding phase volume. Product carbon selectivity was defined as the ratio of carbon moles of product divided by the total carbon moles of corresponding categories (light gases, gasoline-range products, and aqueous-phase products).

Before conducting measurements with different space velocities, the catalysts had been running at a weight hourly space velocity (WHSV) of 0.16 h^{-1} at 518 K for 70 hours. At least three liquid samples were collected for each reaction condition at regular intervals after steady state performance had been attained with time on stream in the gas phase.

3. Results and discussion

3.1. High-throughput studies

3.1.1. Catalyst characterization. Table 1 presents the chemisorption uptake values of the catalysts tested in the HTR. The addition of Ni and Co to the Ru catalyst and Fe to the Ru and Pt catalysts increased the H_2 uptake. The H_2 uptake went through a maximum at Ni/Pt = 1 or Co/Pt = 1 when Ni and Co were added to the Pt catalyst. However, the H_2 uptake of Pd-based bimetallic catalysts was lower than the monometallic Pd catalyst by factors of 2 to 6. Hydrogen can adsorb into bulk Pd metal, causing an overestimation of the number of active sites.^{36–38} We performed CO chemisorption for the Pd-based catalysts to check if hydrogen adsorbs into bulk Pd on the catalysts. The metal dispersion based on the H_2 uptake and the CO uptake was 41.2% and 42.1% respectively, suggesting that hydrogen atoms do not go into the Pd bulk for our catalyst systems. As more Ni and Co were added into the Pd catalyst, the CO uptake decreased, consistent with previous studies.^{39,40} Similar to the H_2 uptake, the CO uptake also decreased as more Fe was added to the Pd catalyst. It is possible that Fe encapsulates Pd metal sites, allowing less H_2 and CO chemisorb on the Pd sites. Shao *et al.* reported that overlaid Pd on Fe has a lower d-band center than Pd.²³ Greeley and

Fig. 1 shows H_2 -TPR of 3 wt% Pd/ $\gamma\text{-Al}_2\text{O}_3$, 5 wt% Fe/ $\gamma\text{-Al}_2\text{O}_3$, and $\text{Pd}_1\text{Fe}_3/\gamma\text{-Al}_2\text{O}_3$ catalysts. Table 2 shows the theoretical hydrogen consumption and the actual hydrogen consumption during reduction for these three catalysts. The 3 wt% Pd catalyst was completely reduced at $<363 \text{ K}$.⁴² The monometallic Fe catalyst started to consume hydrogen at 600 K. Only a small fraction of the Fe was reduced in the Fe/ $\gamma\text{-Al}_2\text{O}_3$ catalyst with a hydrogen consumption of $146.1 \mu\text{mol g}^{-1}$ at 800 K despite a theoretical hydrogen consumption of $1343 \mu\text{mol g}^{-1}$. This indicates that Fe in the Fe/ $\gamma\text{-Al}_2\text{O}_3$ is a mixture of FeO and Fe_2O_3 at a temperature between 600 to 800 K.⁴³ The reduction for the bimetallic Pd-Fe catalyst showed several TPR peaks with the largest peak starting at 363 K. The hydrogen consumption between 363 K and 473 K is $552.1 \mu\text{mol g}^{-1}$ which is 36% of the theoretical hydrogen consumption value. Thus, the existence of Pd metal helps the reduction of iron oxides. It is well

Table 1 Chemisorption data for $\gamma\text{-Al}_2\text{O}_3$ supported monometallic and bimetallic catalysts

Catalyst	H_2 uptake [$\mu\text{mol g}^{-1}$]	CO uptake [$\mu\text{mol g}^{-1}$]
Pd_1Ni_1	21.6	67.5
Pd_1Ni_3	22.5	56.9
Pd_1Co_1	21.8	57.4
Pd_1Co_3	22.9	50.1
Pd_1Fe_1	22.4	42.9
Pd_1Fe_3	10.6	13.2
Pd	58.1	118.6
Ru_1Ni_1	44.8	—
Ru_1Ni_3	81.2	—
Ru_1Co_1	35.5	—
Ru_1Co_3	44.9	—
Ru_1Fe_1	36.5	—
Ru_1Fe_3	34.5	—
Ru	34.3	—
Pt_1Ni_1	56.8	—
Pt_1Ni_3	48.7	—
Pt_1Co_1	51.9	—
Pt_1Co_3	46.4	—
Pt_1Fe_1	56.0	—
Pt_1Fe_3	38.8	—
Pt	37.7	—
Ni	84.7	—
Co	18.1	—

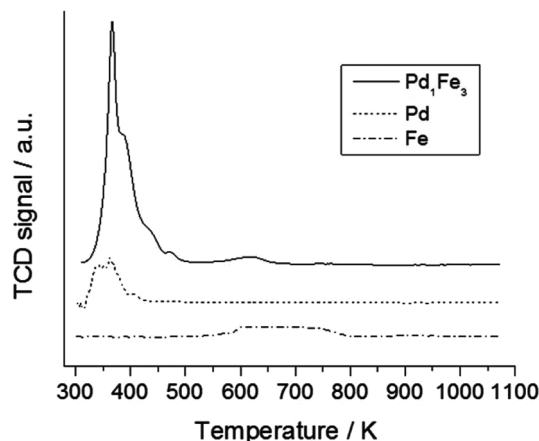


Fig. 1 H₂-TPR patterns of γ -Al₂O₃ supported Pd, Fe, and Pd₁Fe₃ catalysts.

Table 2 H₂ consumption of γ -Al₂O₃ supported Pd, Fe, and Pd₁Fe₃ catalysts determined by H₂-TPR measurements

Catalyst	Theoretical H ₂ consumption ^a [$\mu\text{mol g}^{-1}$]	T_{max} of H ₂ consumption [$\mu\text{mol g}^{-1}$] from TPR		
		<363 K	363–473 K	>573 K
3 wt% Pd	281.9	280.3	0	0
5 wt% Fe	1343.0	0	0	146.1
Pd ₁ Fe ₃	1544.3	0	552.1	25.2

^aTheoretical H₂ consumption assuming the metal oxides are completely reduced to their metallic states.

known that the addition of a noble metal into Fe catalyst increases the reducibility of iron oxides.^{44–47}

3.1.2. High-throughput screening of bimetallic catalysts for aqueous-phase hydrogenation of propanal, xylose, and furfural. We previously showed that Ru was the most active monometallic catalyst for APH of propanal and xylose.¹⁰ The activity of monometallic catalysts for APH of furfural decreased in the order: Pd ~ Ni > Co > Ru > Pt > Rh.¹⁰ We also showed that the rate of propanal hydrogenation is 3 times faster than furfural hydrogenation, demonstrating that steric effects are important for APH of carbonyl groups.¹⁰ The focus of the HTR screening study is to elucidate activity trends for hydrogenation of different carbonyl compounds with different bimetallic catalysts. Table 3 summarizes the reaction rates for APH of propanal, xylose, and furfural over different monometallic and bimetallic catalysts in the HTR.

The Pd-bimetallic catalysts were up to 63 times more active than the monometallic Pd catalyst for propanal hydrogenation. The bimetallic catalyst activity for propanal hydrogenation decreased as Pd–Fe > Pd–Ni > Pd–Co. The Pd–Fe and Pd–Ni catalysts had the highest activity for propanal hydrogenation at a base metal to Pd molar ratio of 3 : 1 (Pd₁Fe₃ and Pd₁Ni₃). In contrast, the Pd–Co catalyst had the highest activity for propanal hydrogenation at a Co to Pd molar ratio of 1 : 1 (Pd₁Co₁). The Pd₁Fe₃ catalyst is the most active catalyst tested for APH of

propanal, 63 times higher than the rate of the 3 wt% Pd catalyst.

The 3 wt% Ru catalyst was the most active monometallic catalyst for APH of propanal with a hydrogenation rate of 1810 h^{–1}. The Ru₁Co₁ catalyst had the highest hydrogenation rate for propanal conversion among all Ru bimetallic catalysts tested in this study. Based on a statistical student *t*-test, the addition of Fe to the monometallic Ru catalyst did not significantly enhance the rate of propanal hydrogenation. Ni addition at a Ni/Ru = 1 level (Ru₁Ni₁) also did not statistically show any significant difference in the rate of propanal hydrogenation compared to the pure Ru catalyst. Further addition of Ni to form the Ru₁Ni₃ catalyst, decreased the catalytic activity for propanal hydrogenation to levels below that of the monometallic Ru catalyst.

Addition of Ni, Co, and Fe to the monometallic Pt catalyst increased the rate of propanal hydrogenation. The maximum rate for all three of these bimetallic catalysts was observed at a base metal to Pt molar ratio of 3 to 1. The Pt₁Co₃ catalyst was very active for APH of propanal with a rate of 5160 h^{–1}. The Pt₁Fe₃ catalyst had a rate of 4700 h^{–1} for propanal hydrogenation that was 14 times more active than the monometallic Pt catalyst. The Pt₁Ni₃ catalyst showed propanal hydrogenation rate 8 times as high as the 3 wt% Pt catalyst. The results of Pt–Co bimetallic catalysts being more active for APH of propanal are consistent with the work of Zheng *et al.* who showed that a Co–Pt bimetallic catalyst is more active than the parent monometallic catalysts (Pt and Co) for hydrogenation of acetaldehyde and acetone.¹² They concluded the increase in activity was because acetaldehyde and acetone adsorbed more weakly on Pt–Co–Pt(111) bimetallic surface than the parent monometallic surfaces (Pt(111) and Co(0001)).¹²

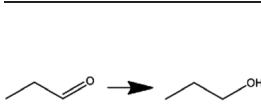
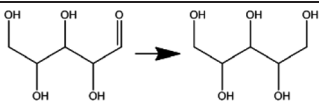
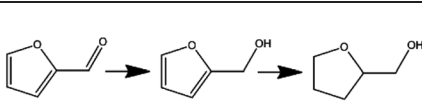
The monometallic Ru catalyst was the most active catalyst for APH of xylose among all catalysts tested in the HTR. The addition of Ni, Co, and Fe to the Ru catalyst decreased the activity of the Ru catalyst for xylose hydrogenation.

The addition of Ni, Co, and Fe to the monometallic Pd catalyst increased the activity for APH of xylose where each catalyst had a maximum rate at a base metal to Pd molar ratio of 3 to 1. The order of decreasing activity for xylose hydrogenation decreased as Pd–Ni > Pd–Fe ~ Pd–Co. The Pd₁Ni₃ catalyst was 110 times more active than the monometallic Pd catalyst for APH of xylose. The Pd₁Fe₃ catalyst had a 50 times higher reaction rate than the monometallic Pd catalyst for xylose hydrogenation.

The addition of Ni, Co, and Fe to the monometallic Pt catalyst increased the activity for APH of xylose with the bimetallic activity decreasing as Pt–Ni > Pt–Co > Pt–Fe. The Pt₁Ni₃ catalyst was 16 times more active than the monometallic Pt catalyst.

The products observed from APH of furfural were furfuryl alcohol and THFA. Addition of Fe and Co to the Pd catalyst increased the activity of the Pd for APH of furfural. The Pd–Fe bimetallic catalysts were the most active catalysts for APH of furfural. The Pd₁Fe₃ catalyst was 9 times more active than the monometallic Pd catalyst for APH of furfural. The Pd–Co bimetallic catalysts were up to 40% more active than the

Table 3 Reaction rate and standard error for APH of propanal, xylose, and furfural over γ - Al_2O_3 supported monometallic and bimetallic catalysts. Reaction conditions: 373 K, 5.41 MPa, 5 wt% propanal, 5 wt% xylose, and 4.8 wt% furfural solutions as the feed

Catalyst	Reaction rate (h^{-1})		
			
Pd_1Ni_1	994.7 (± 76.4)	885.2 (± 69.7)	504.5 (± 49.7)
Pd_1Ni_3	1541.0 (± 135.1)	1552.0 (± 145.4)	329.7 (± 30.4)
Pd_1Co_1	894.5 (± 69.8)	101.1 (± 10.7)	1107.2 (± 105.8)
Pd_1Co_3	586.5 (± 38.5)	724.7 (± 73.9)	675.1 (± 63.4)
Pd_1Fe_1	1234.6 (± 88.6)	109.2 (± 10.5)	2147.3 (± 210.1)
Pd_1Fe_3	6387.3 (± 601.2)	701.3 (± 57.0)	4677.4 (± 417.2)
3 wt% Pd	100.6 (± 7.2)	13.8 (± 2.4)	459.9 (± 34.4)
Ru_1Ni_1	2021.0 (± 118.0)	1255.4 (± 106.0)	206.6 (± 18.0)
Ru_1Ni_3	1293.5 (± 119.7)	880.2 (± 75.2)	164.7 (± 15.2)
Ru_1Co_1	3386.8 (± 149.4)	1735.7 (± 165.7)	545.9 (± 55.7)
Ru_1Co_3	2180.1 (± 126.3)	1160.4 (± 103.7)	398.3 (± 33.7)
Ru_1Fe_1	2026.8 (± 205.7)	899.7 (± 60.5)	537.2 (± 50.5)
Ru_1Fe_3	2046.3 (± 209.1)	705.8 (± 53.7)	581.4 (± 33.7)
3 wt% Ru	1811.6 (± 122.1)	2476.9 (± 208.8)	204.3 (± 20.1)
Pt_1Ni_1	1969.9 (± 158.1)	409.1 (± 36.4)	73.2 (± 7.3)
Pt_1Ni_3	2458.2 (± 209.8)	872.7 (± 85.1)	282.9 (± 18.4)
Pt_1Co_1	2865.1 (± 224.0)	206.0 (± 19.8)	199.1 (± 12.3)
Pt_1Co_3	5162.7 (± 455.4)	390.1 (± 28.5)	427.2 (± 41.3)
Pt_1Fe_1	2447.9 (± 209.4)	158.9 (± 13.6)	214.4 (± 16.4)
Pt_1Fe_3	4701.6 (± 442.6)	200.2 (± 20.2)	828.1 (± 48.5)
3 wt% Pt	320.4 (± 13.0)	51.3 (± 6.2)	48.8 (± 3.8)
20 wt% Ni	818.8 (± 78.1)	333.0 (± 30.4)	277.0 (± 20.4)
20 wt% Co	111.5 (± 7.1)	196.0 (± 18.6)	78.0 (± 6.6)
20 wt% Fe	0	0	0

monometallic Pd catalyst. The Pd_1Ni_3 bimetallic catalyst was less active than the 3 wt% Pd catalyst even though Pd and Ni are both very active metals for APH of furfural.

The addition of Fe and Co to the monometallic Ru catalyst increased the activity up to 2 times for APH of furfural. Ni addition to the monometallic Ru catalyst decreased the activity by 19%. The addition of Ni, Co, and Fe to the Pt catalyst increased the rate for furfural hydrogenation with the most active bimetallic catalysts being Pt–Fe. The Pt_1Fe_3 catalyst was 16 times more active than the 3 wt% Pt catalyst for furfural hydrogenation. The Pt_1Co_3 catalyst was 9 times as active as the 3 wt% Pt catalyst for APH of furfural. The Pt_1Ni_1 catalyst had a higher hydrogenation rate than the 3 wt% Pt catalyst but a lower hydrogenation rate than the 20 wt% Ni catalyst.

The Pd-based bimetallic catalysts produced both furfuryl alcohol (88.5 to 93.1%) and THFA (6.9 to 11.5%) from furfural. This indicates that the Pd-based bimetallic catalysts are also active in the hydrogenation of the C=C bond in a furan ring. The Ru-based bimetallic catalysts made THFA with small portions (0.2 to 3.6%). The Pt-based bimetallic catalysts produced only furfuryl alcohol.

The results from APH of different carbonyl compounds performed in the HTR demonstrate that the Fe promoted Pd catalyst (*i.e.* Pd_1Fe_3) is the most active catalyst for propanal and furfural hydrogenation and also very active for xylose hydrogenation (Fig. 2), suggesting that Fe addition to Pd catalyst could increase the activity for hydrogenation of carbonyl compounds. One hypothesis is that the Fe in Pd–Fe bimetallic

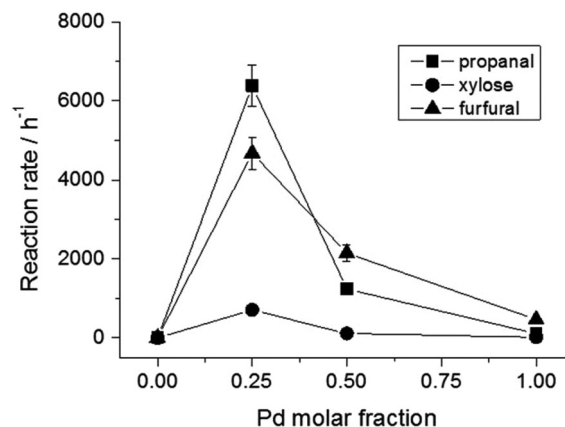


Fig. 2 Reaction rate for APH of propanal, xylose, and furfural as a function of Pd molar fraction in Pd–Fe catalysts. Reaction conditions: 373 K, 5.41 MPa, 5 wt% propanal, 5 wt% xylose, and 4.8 wt% furfural solutions as the feed.

surface decreases the binding energy of the carbonyl group, resulting in a higher activity for hydrogenation of carbonyl groups.^{12,13}

On the Pd_1Fe_3 catalyst the hydrogenation rate for each molecule decreases in the order: propanal > furfural > xylose. For xylose hydrogenation, the O atom on the carbonyl group adsorbs on a catalyst surface through O along with an adsorption of O atom on the hydroxyl group adjacent to the carbonyl group on the catalyst surface.⁴⁸ This adsorbed O atom of the

hydroxyl group may prevent hydrogenation of C=O bond of xylose. However, for propanal and furfural, the carbonyl group adsorbs on Pd metal surface through both C and O.^{25,49} For propanal hydrogenation, the adsorbed carbonyl species is hydrogenated to form a surface alkoxide species *via* the addition of adsorbed H to the adsorbed O atom.^{25,50,51} In contrast to propanal, a hydroxyalkyl surface species is the dominant intermediate through H addition to C atom due to the conjugation with the furan ring of furfural.^{25,52} Atomic O is more electronegative than atomic C; hence, the alkoxide intermediate can more easily react with H than the hydroxyalkyl intermediate resulting in higher activity for hydrogenation of propanal than of furfural.

3.2. Aqueous-phase hydrodeoxygenation of sorbitol over Pd/Zr-P and Pd-Fe/Zr-P

From the high-throughput screening, we found that the addition of Fe to Pd increases the activity up to 63 times for hydrogenation of a carbonyl group. The hydrogenation of carbonyl groups is an important fundamental reaction in HDO of biomass-derived oxygenates.^{3,53,54} The carbonyl groups are produced during HDO by several routes including: (1) dehydration of alcohols or polyols and (2) C-C bond cleavage reactions.⁵³ For instance, ethylene glycol is produced from hydrogenation of 2-hydroxyacetaldehyde which is produced through dehydrogenation and retro-aldol condensation of sorbitol.⁵³ Previously Pd catalyst has been shown to have lower activity but higher hexane selectivity than Pt for aqueous-phase HDO of sorbitol.³ Pd is also 55% cheaper than Pt.⁵⁵ Hence, our high-throughput studies suggest one option to increase the activity of Pd catalysts for HDO of sorbitol would be to add Fe to the Pd catalyst. HDO reaction occurs through a bifunctional reaction pathway on metal-acid catalysts. Zr-P is one of the most promising solid-acids for HDO for this reaction because it has a high Brønsted to Lewis acid ratio, is hydrothermally stable, and does not leach during the reaction.^{56,57} Therefore, we synthesized a Pd₁Fe₃/Zr-P catalyst and carried out HDO of sorbitol on the Pd₁Fe₃/Zr-P catalyst in a continuous flow reactor.

Table 4 lists the BET surface area and H₂ uptake of the 3 wt% Pd/Zr-P and Pd₁Fe₃/Zr-P catalysts before and after reaction. During the reaction both catalysts underwent phase transformation from an amorphous material to a crystalline material as shown by XRD in Fig. S1.† Both catalysts lost BET and metal surface area after reaction. This is similar to results

Table 4 BET surface area and H₂ chemisorption data of Pd/Zr-P and Pd-Fe/Zr-P before and after reaction. Reaction conditions: 518 K, 6.21 MPa, 20 wt% sorbitol solution as the feed, and flow rate of H₂ is 40 mL min⁻¹

Catalyst	S _{BET} [m ² g ⁻¹]	H ₂ uptake [μmol g ⁻¹]
3 wt% Pd/Zr-P	238.0	19.3
3 wt% Pd/Zr-P after reaction	19.7	1.1
Pd ₁ Fe ₃ /Zr-P	102.3	16.4
Pd ₁ Fe ₃ /Zr-P after reaction	6.7	0.2

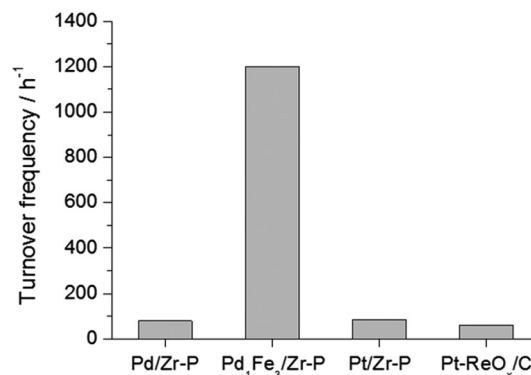


Fig. 3 TOF for HDO of sorbitol over Pd/Zr-P, Pd₁Fe₃/Zr-P, Pt/Zr-P, and Pt-ReO_x/C. The TOF of Pt/Zr-P and Pt-ReO_x/C is from the literature.⁵⁸ Reaction conditions: 518 K, 6.21 MPa, 20 wt% sorbitol solution as the feed, and flow rate of H₂ is 40 mL min⁻¹.

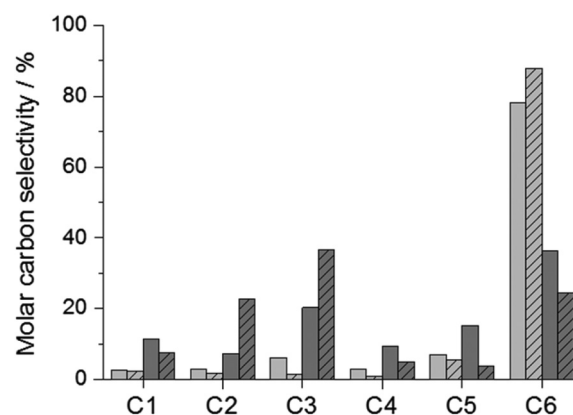


Fig. 4 Molar carbon selectivity of C1–C6 products (normalized without polymerized humins) over Pd/Zr-P (light gray) and Pd-Fe/Zr-P (dark gray) for HDO of sorbitol. Reaction conditions: 518 K, 6.21 MPa, WHSV = 0.16 h⁻¹ (no pattern in bars) and 2.92 h⁻¹ (pattern in bars), 20 wt% sorbitol solution as the feed, and flow rate of H₂ is 40 mL min⁻¹.

obtained with Pt/Zr-P.⁵⁸ However, in spite of the loss of surface area, both catalysts were stable as shown by the time on stream data in Fig. S2.†

The Pd₁Fe₃/Zr-P was the most active catalyst we have tested for HDO of sorbitol, as shown in Fig. 3.^{53,58,59} The TOF of the Pd₁Fe₃/Zr-P (based on H₂ uptake after reaction) was 14 times higher than the TOF of the Pd/Zr-P. The Pd₁Fe₃/Zr-P catalyst was 13 times more active than a Pt/Zr-P catalyst⁵⁸ and 18 times more active than a Pt-ReO_x/C catalyst.⁵⁸ This suggests that the hydrogenation of carbonyl groups is a kinetically slow step on Pd catalysts and carbonyl intermediates may poison the Pd catalyst surface.^{60–62}

Fig. 4 shows that the C6 product selectivity decreased and the C1–C4 products selectivity increased by Fe addition to the Pd catalyst. Even at the low conversion (WHSV = 2.92 h⁻¹), the Pd₁Fe₃/Zr-P catalyst had a higher selectivity toward C1–C4 products than the Pd/Zr-P. The Pd₁Fe₃/Zr-P catalyst produced more ethylene glycol, propylene glycol, and glycerol than the Pd/Zr-P, as shown in Table 5. This indicates that

Table 5 Molar carbon selectivity of products in gas and liquid phases over Pd/Zr-P and Pd-Fe/Zr-P for HDO of sorbitol. Reaction conditions: 518 K, 6.21 MPa, 20 wt% sorbitol solution as the feed, and flow rate of H₂ is 40 mL min⁻¹

Catalyst	3 wt% Pd/Zr-P		Pd ₁ Fe ₃ /Zr-P	
WHSV (h ⁻¹)	0.16	2.92	0.16	2.92
Conversion (%)	97.8	5.1	100	15.9
Reaction rate (μmol _{sorbitol} g _{cat} ⁻¹ s ⁻¹)		0.05		0.14
TOF (h ⁻¹)	—	79.1	—	1200.0
Alcohol selectivity (%)				
Methanol	0.4	0.5	1.0	1.9
Ethanol	0.5	0	3.8	1.7
1-Propanol	2.8	0.3	11.3	0.4
2-Propanol	0.02	0	0.4	0
1-Butanol	0.4	0	1.6	0.02
2-Butanol	0	0	0.3	0
1-Pentanol	0.1	0	0.8	0
2-Pentanol	0.1	0	0.2	0
1-Hexanol	1.1	0.3	1.6	0.1
2-Hexanol	0.02	0	0.1	0
3-Hexanol	0.3	0	0.3	0
Total alcohols	5.9	1.1	21.3	4.1
Aldehyde selectivity (%)				
Butanal	0.1	0.4	0.1	1.1
Pentanal	0	0	0.6	0
Total aldehydes	0.1	0.4	0.7	1.1
Ketone selectivity (%)				
Acetone	0.03	0	0.7	0
Hydroxyacetone	0	0	0.2	8.0
2-Butanone	0.1	0	1.3	0
2-Pentanone	0.1	0	0.4	0
3-Pentanone	1.0	0.5	0.9	0
2-Hexanone	0.1	0	0.3	0
3-Hexanone	0.1	0	0.6	0
Total ketones	1.4	0.5	4.4	8.0
Alkanediol selectivity (%)				
Ethylene glycol	1.1	1.3	0.3	20.0
Propylene glycol	0.1	0.8	1.1	24.8
1,2-Butanediol	0	0	0.4	2.3
1,4-Butanediol	0.1	0	0.3	0
2,3-Butanediol	0	0	1.0	1.3
1,2-Pentanediol	0.4	1.1	0.6	0
1,4-Pentanediol	0.04	0.4	0.5	0.5
1,5-Pentanediol	0.1	0.2	0.1	0
1,2-Hexanediol	0	0	0	0
1,6-Hexanediol	0.1	1.2	0.1	0
2,5-Hexanediol	0	0	0.7	0
Total alkanediols	1.9	4.9	5.1	49.1
Polyol selectivity (%)				
Glycerol	0.2	0	0.3	1.8
1,2,6-Hexanetriol	0.1	0	0.02	0.7
Mannitol	3.0	0	0	0
Total polyols	3.3	0	0.3	2.5
Heterocyclic compound selectivity (%)				
Tetrahydrofuran	0.4	0.2	0.6	0
3-Hydroxy-tetrahydrofuran	0.1	0	0.8	0
2-Methyl-tetrahydrofuran	0.3	0.3	0.7	0
5-Hydroxymethylfurfural	0	0	0	0.1
Tetrahydrofurfuryl alcohol	0.8	1.0	2.7	1.9
Tetrahydropyran	0.7	0	1.1	0
Tetrahydro-4H-pyran-4-ol	0.3	0.7	0.9	0.1
2,5-Dimethyltetrahydrofuran	2.5	4.7	1.7	1.7
5-Methyltetrahydrofuran-2-methanol	1.4	2.2	3.2	0.7
Tetrahydro-2-methoxymethyl-furan	0.7	1.0	2.2	1.0
2-Methyl-tetrahydropyran	3.4	2.8	2.8	2.4
Tetrahydropyran-2-methanol	5.0	0.9	9.5	0.2
Cyclopentanone	0	0	0.1	1.1
1,2-Cyclohexanediol	0	0	0	0
Isosorbide	26.8	42.7	2.0	14.2
Sorbitan	3.0	9.6	0.6	1.0
Total heterocyclic compounds	45.5	65.9	29.0	24.2

Table 5 (Contd.)

Carboxylic acid selectivity (%)				
Propanoic acid	0.3	0	0.5	0
Butyric acid	0.1	0	0.2	0
Pentanoic acid	0.2	0	0.3	0.04
Hexanoic acid	0.2	0.6	0.6	1.2
Total carboxylic acids	0.8	0.6	1.6	1.3
Alkane selectivity (%)				
Methane	0.05	0.02	0.6	0.02
Ethane	0.2	0.1	1.4	0.01
Propane	0.5	0.1	0.8	0
Butane	0.5	0.2	0.4	0
Pentane	0.2	0.1	0.5	0.01
Hexane	1.0	0.8	0.5	0.01
Total alkanes	2.5	1.3	4.2	0.04
CO selectivity (%)	0.6	0.2	1.5	0.3
CO ₂ selectivity (%)	0.7	1.0	5.4	5.0
Humins (%)	36.5	1.2	24.1	0.3

the addition of Fe to the Pd catalyst promotes C–C bond cleavage (dehydrogenation/retro-aldol condensation) compared to the monometallic Pd and Pt⁵⁸ catalysts. This might be due to interactions between Fe-containing bimetallic sites and FeO species existing on the periphery of the bimetallic sites.⁶³

Table 5 shows the detailed product selectivity for each catalyst on a molar carbon basis grouped by product functionality. Only trace amounts of aldehydes were detected for both catalysts, indicating that aldehydes rapidly converted to their corresponding alcohols on the Pd and Pd–Fe catalysts. There were up to 7 times more ketones than aldehydes in the liquid phase. We observed that aldehyde hydrogenation was up to 58% faster than ketone hydrogenation on Pd catalysts.¹⁰ The Pd₁Fe₃/Zr–P also had a lower selectivity toward sorbitan and isosorbide that are made through dehydration of sorbitol at acid sites of Zr–P than the Pd/Zr–P (Table 5). By adding Fe to the Pd catalyst, the C₆ alcohols, C₆ diols, C₆ polyols, and C₆ cyclic ethers selectivity increased from 16% to 24.3% at WHSV = 0.16 h^{−1}. This suggests that the addition of Fe to the Pd catalyst promotes the conversion of sorbitan and isosorbide through a series of dehydration/hydrogenation (or hydrogenolysis) reactions. At the high conversion (WHSV = 0.16 h^{−1}) for both catalysts we observed a white insoluble product in the liquid phase that we report as humins in Table 5. The humins were probably formed *via* polymerization of isosorbide.⁶⁴

In Table S2,† we grouped the products into three categories: (1) light gases such as C₁–C₄ alkanes and CO₂, (2) gasoline-range products including C₅–C₆ alkanes, C₂–C₆ monofunctional compounds (including alcohols, aldehydes, cyclic ethers, carboxylic acids, and ketones), and (3) aqueous-phase oxygenates including methanol, polyols, mannitol, sorbitan, and isosorbide.^{59,65} The Pd₁Fe₃/Zr–P had a higher yield (55.1%) of gasoline-range products than the 3 wt% Pd/Zr–P (24.1%). The estimated research octane number (RON) of the Pd₁Fe₃/Zr–P (101.3) was also higher than the RON of the Pd/Zr–P (92.2) at WHSV = 0.16 h^{−1}.

4. Conclusions

The addition of Ni, Co, or Fe to the monometallic Pd and Pt catalysts usually increased the activity for APH of propanal and furfural. In contrast, all bimetallic catalysts tested in this study had a lower activity than the monometallic Ru catalyst for APH of xylose. The reaction rate for APH of propanal increased by the addition of Ni, Co, and Fe to the monometallic Pd catalyst with the bimetallic Pd₁Fe₃ catalyst being most active for APH of propanal. The addition of Fe to the monometallic Pd catalyst increased the reaction rate for APH of xylose by a factor of 51. The Pd₁Fe₃ bimetallic catalyst had the highest activity for APH of furfural. The Pd-based bimetallic catalysts produced not only furfuryl alcohol but also THFA for APH of furfural, meaning that the Pd-based bimetallic catalysts are also active not only for C=O bond hydrogenation but also for C=C bond hydrogenation. The Pd₁Fe₃ bimetallic catalyst was used for HDO of sorbitol with Zr–P as a support. The Pd₁Fe₃/Zr–P catalyst was the most active catalyst we have tested for HDO of sorbitol. The addition of Fe to the Pd enhanced C–C bond cleavage and C–O hydrogenolysis reactions. Moreover, Fe addition to the Pd increased the conversion of sorbitan and isosorbide to C₆ alcohols, C₆ diols, C₆ polyols, and C₆ cyclic ethers. The Pd₁Fe₃/Zr–P was also more selective to gasoline-range products than the Pd/Zr–P.

Acknowledgements

This material is based upon work supported as part of the Institute for Atom-efficient Chemical Transformations (IACT), an Energy Frontier Research Center funded by the U.S. Department of Energy, Office of Science, Office of Basic Energy Sciences.

References

- 1 J. W. Shabaker, G. W. Huber, R. R. Davda, R. D. Cortright and J. A. Dumesic, *Catal. Lett.*, 2003, **88**, 1–8.

- 2 R. R. Davda, J. W. Shabaker, G. W. Huber, R. D. Cortright and J. A. Dumesic, *Appl. Catal., B*, 2003, **43**, 13–26.
- 3 G. W. Huber, R. D. Cortright and J. A. Dumesic, *Angew. Chem., Int. Ed.*, 2004, **43**, 1549–1551.
- 4 R. R. Davda, J. W. Shabaker, G. W. Huber, R. D. Cortright and J. A. Dumesic, *Appl. Catal., B*, 2005, **56**, 171–186.
- 5 G. W. Huber, J. N. Chheda, C. J. Barrett and J. A. Dumesic, *Science*, 2005, **308**, 1446–1450.
- 6 G. W. Huber and J. A. Dumesic, *Catal. Today*, 2006, **111**, 119–132.
- 7 J. N. Chheda and J. A. Dumesic, *Catal. Today*, 2007, **123**, 59–70.
- 8 J. N. Chheda, G. W. Huber and J. A. Dumesic, *Angew. Chem., Int. Ed.*, 2007, **46**, 7164–7183.
- 9 H. Olcay, L. J. Xu, Y. Xu and G. W. Huber, *ChemCatChem*, 2010, **2**, 1420–1424.
- 10 J. Lee, Y. Xu and G. W. Huber, *Appl. Catal., B*, 2013, **140–141**, 98–107.
- 11 D. M. Alonso, S. G. Wettstein and J. A. Dumesic, *Chem. Soc. Rev.*, 2012, **41**, 8075–8098.
- 12 R. Y. Zheng, Y. X. Zhu and J. G. G. Chen, *ChemCatChem*, 2011, **3**, 578–581.
- 13 R. Y. Zheng, M. P. Humbert, Y. X. Zhu and J. G. Chen, *Catal. Sci. Technol.*, 2011, **1**, 638–643.
- 14 Y. Nakagawa and K. Tomishige, *Catal. Commun.*, 2010, **12**, 154–156.
- 15 G. W. Huber, J. W. Shabaker, S. T. Evans and J. A. Dumesic, *Appl. Catal., B*, 2006, **62**, 226–235.
- 16 J. C. Bertolini, B. Tardy, M. Abon, J. Billy, P. Delichere and J. Massardier, *Surf. Sci.*, 1983, **135**, 117–127.
- 17 H. Igarashi, T. Fujino, Y. M. Zhu, H. Uchida and M. Watanabe, *Phys. Chem. Chem. Phys.*, 2001, **3**, 306–314.
- 18 E. Christoffersen, P. Liu, A. Ruban, H. L. Skriver and J. K. Nørskov, *J. Catal.*, 2001, **199**, 123–131.
- 19 J. Greeley and M. Mavrikakis, *Nat. Mater.*, 2004, **3**, 810–815.
- 20 A. U. Nilekar, Y. Xu, J. L. Zhang, M. B. Vukmirovic, K. Sasaki, R. R. Adzic and M. Mavrikakis, *Top. Catal.*, 2007, **46**, 276–284.
- 21 W. P. Zhou, X. F. Yang, M. B. Vukmirovic, B. E. Koel, J. Jiao, G. W. Peng, M. Mavrikakis and R. R. Adzic, *J. Am. Chem. Soc.*, 2009, **131**, 12755–12762.
- 22 V. R. Stamenkovic, B. S. Mun, M. Arenz, K. J. J. Mayrhofer, C. A. Lucas, G. F. Wang, P. N. Ross and N. M. Markovic, *Nat. Mater.*, 2007, **6**, 241–247.
- 23 M. H. Shao, P. Liu, J. L. Zhang and R. Adzic, *J. Phys. Chem. B*, 2007, **111**, 6772–6775.
- 24 H. J. Kim, S. M. Choi, M. H. Seo, S. Green, G. W. Huber and W. B. Kim, *Electrochem. Commun.*, 2011, **13**, 890–893.
- 25 S. Sitthitha, T. Pham, T. Prasomsri, T. Sooknoi, R. G. Mallinson and D. E. Resasco, *J. Catal.*, 2011, **280**, 17–27.
- 26 S. Sitthitha, W. An and D. E. Resasco, *J. Catal.*, 2011, **284**, 90–101.
- 27 P. T. M. Do, A. J. Foster, J. G. Chen and R. F. Lobo, *Green Chem.*, 2012, **14**, 1388–1397.
- 28 G. W. Huber, J. W. Shabaker and J. A. Dumesic, *Science*, 2003, **300**, 2075–2077.
- 29 S. Senkan, K. Krantz, S. Ozturk, V. Zengin and I. Onal, *Angew. Chem., Int. Ed.*, 1999, **38**, 2794–2799.
- 30 R. J. Hendershot, S. S. Lasko, M. F. Fellmann, G. Oskarsdottir, W. N. Delgass, C. M. Snively and J. Lauterbach, *Appl. Catal., A*, 2003, **254**, 107–120.
- 31 P. Serna, L. A. Baumes, M. Moliner and A. Corma, *J. Catal.*, 2008, **258**, 25–34.
- 32 L. A. Baumes, P. Serna and A. Corma, *Appl. Catal., A*, 2010, **381**, 197–208.
- 33 I. Onal, D. Duzenli, A. Seubsai, M. Kahn, E. Seker and S. Senkan, *Top. Catal.*, 2010, **53**, 92–99.
- 34 S. K. Green, J. Lee, H. J. Kim, G. A. Tompsett, W. B. Kim and G. W. Huber, *Green Chem.*, 2013, **15**, 1869–1879.
- 35 Y. Kamiya, S. Sakata, Y. Yoshinaga, R. Ohnishi and T. Okuhara, *Catal. Lett.*, 2004, **94**, 45–47.
- 36 F. A. Lewis, *Platinum Metals Rev.*, 1960, **4**, 132–137.
- 37 F. D. Manchester, A. San-Martin and J. M. Pitre, *J. Phase Equilib.*, 1994, **15**, 62–83.
- 38 G. Fagherazzi, A. Benedetti, S. Polizzi, A. Dimario, F. Pinna and M. Signoretto, *Catal. Lett.*, 1995, **32**, 293–303.
- 39 A. Sarkany, Z. Zsoldos, G. Stefler, J. W. Hightower and L. Gucci, *J. Catal.*, 1995, **157**, 179–189.
- 40 N. S. Babu, N. Lingaiah and P. S. S. Prasad, *Appl. Catal., B*, 2012, **111**, 309–316.
- 41 J. Greeley and M. Mavrikakis, *J. Phys. Chem. B*, 2005, **109**, 3460–3471.
- 42 L. L. Cai, G. Z. Lu, W. C. Zhan, Y. Guo, Y. L. Guo, Q. S. Yang and Z. G. Zhang, *J. Mater. Sci.*, 2011, **46**, 5639–5644.
- 43 H.-J. Wan, B.-S. Wu, C.-H. Zhang, H.-W. Xiang, Y.-W. Li, B.-F. Xu and F. Yi, *Catal. Commun.*, 2007, **8**, 1538–1545.
- 44 L. Gucci, *Catal. Rev. Sci. Eng.*, 1981, **23**, 329–376.
- 45 D. Richard, J. Ockelford, A. Giroirfendler and P. Gallezot, *Catal. Lett.*, 1989, **3**, 53–58.
- 46 F. J. Berry, C. H. Xu and S. Jobson, *J. Chem. Soc., Faraday Trans.*, 1990, **86**, 165–169.
- 47 J. Xu, C. H. Bartholomew, J. Sudweeks and D. L. Eggett, *Top. Catal.*, 2003, **26**, 55–71.
- 48 M. Yadav, D. K. Mishra and J.-S. Hwang, *Appl. Catal., A*, 2012, **425–426**, 110–116.
- 49 M. Mavrikakis and M. A. Barteau, *J. Mol. Catal. A: Chem.*, 1998, **131**, 135–147.
- 50 R. Alcalá, J. Greeley, M. Mavrikakis and J. A. Dumesic, *J. Chem. Phys.*, 2002, **116**, 8973–8980.
- 51 G. M. R. van Druten and V. Ponec, *Appl. Catal., A*, 2000, **191**, 163–176.
- 52 S. Sitthitha, T. Sooknoi, Y. G. Ma, P. B. Balbuena and D. E. Resasco, *J. Catal.*, 2011, **277**, 1–13.
- 53 N. Li and G. W. Huber, *J. Catal.*, 2010, **270**, 48–59.
- 54 B. M. Moreno, N. Li, J. Lee, G. W. Huber and M. T. Klein, *RSC Adv.*, 2013, **3**, 23769–23784.
- 55 Mineral commodity summaries 2012, U.S. Geological Survey, 2012.

- 56 R. Weingarten, G. A. Tompsett, W. C. Conner and G. W. Huber, *J. Catal.*, 2011, **279**, 174–182.
- 57 R. Weingarten, Y. T. Kim, G. A. Tompsett, A. Fernández, K. S. Han, E. W. Hagaman, W. C. Conner Jr., J. A. Dumesic and G. W. Huber, *J. Catal.*, 2013, **304**, 123–134.
- 58 Y. T. Kim, J. A. Dumesic and G. W. Huber, *J. Catal.*, 2013, **304**, 72–85.
- 59 N. Li, G. A. Tompsett and G. W. Huber, *ChemSusChem*, 2010, **3**, 1154–1157.
- 60 F. Delbecq and P. Sautet, *J. Catal.*, 1995, **152**, 217–236.
- 61 M. Burgener, R. Wirz, T. Mallat and A. Baiker, *J. Catal.*, 2004, **228**, 152–161.
- 62 P. Maki-Arvela, J. Hajek, T. Salmi and D. Y. Murzin, *Appl. Catal., A*, 2005, **292**, 1–49.
- 63 B. D. Li, J. Wang, Y. Z. Yuan, H. Ariga, S. Takakusagi and K. Asakura, *ACS Catal.*, 2011, **1**, 1521–1528.
- 64 A. Yamaguchi, N. Hiyoshi, O. Sato and M. Shirai, *Green Chem.*, 2011, **13**, 873–881.
- 65 N. Li, G. A. Tompsett, T. Y. Zhang, J. A. Shi, C. E. Wyman and G. W. Huber, *Green Chem.*, 2011, **13**, 91–101.